Photonuclear reactions with zinc

Boztosun, I.; Dapo, H.; Karakoc, M.; Ozmen, S. F.; Cecen, Y.; Coban, A.; Caner, T.; Bayram, E.; Saito, T. R.; Akdogan, T.

Published in:
European physical journal plus

DOI:
10.1140/epjp/i2015-15185-2

Publication date:
2015

Eur. Phys. J. Plus (2015) **130**: 185
DOI 10.1140/epjp/i2015-15185-2

THE EUROPEAN PHYSICAL JOURNAL PLUS

Regular Article

Photonuclear reactions with zinc: A case for clinical linacs

I. Boztosun[1,2], H. Đapo[1,2,a], M. Karakoç[1,2], S.F. Özmen[1,2], Y. Çeçen[2,3], A. Çoban[1,2], T. Caner[1,2], E. Bayram[4], T.R. Saito[5,6,7], T. Akdoğan[8], V. Bozkurt[9], Y. Kuçuk[1,2], D. Kaya[1,2], and M.N. Harakeh[10]

[1] Department of Physics, Akdeniz University, TR-07058, Antalya, Turkey
[2] Nuclear Research and Application Center, Akdeniz University, TR-07058, Antalya, Turkey
[3] Department of Radiation Oncology, Akdeniz University, TR-07058, Antalya, Turkey
[4] Department of Chemistry, Akdeniz University, TR-07058, Antalya, Turkey
[5] GSI Helmholtz Center for Heavy Ion Research, Planckstrasse 1, 64291 Darmstadt, Germany
[6] Johannes Gutenberg-Universität Mainz, J.J.Becherweg 40, 55099 Mainz, Germany
[7] The Helmholtz Institute Mainz (HIM), J.J.Becherweg 40, 55099 Mainz, Germany
[8] Department of Physics, Bogazici University, 34342 Istanbul, Turkey
[9] Nigde University, 51100 Nigde, Turkey
[10] KVI-CART, University of Groningen, 9747 AA Groningen, The Netherlands

Received: 4 June 2015 / Revised: 14 August 2015
Published online: 14 September 2015 –

Abstract. The use of bremsstrahlung photons produced by a linac to induce photonuclear reactions is wide spread. However, using a clinical linac to produce the photons is a new concept. We aimed to induce photonuclear reactions on zinc isotopes and measure the subsequent transition energies and half-lives. For this purpose, a bremsstrahlung photon beam of 18 MeV endpoint energy produced by the Philips SLI-25 linac has been used. The subsequent decay has been measured with a well-shielded single HPGe detector. The results obtained for transition energies are in good agreement with the literature data and in many cases surpass these in accuracy. For the half-lives, we are in agreement with the literature data, but do not achieve their precision. The obtained accuracy for the transition energies show what is achievable in an experiment such as ours. We demonstrate the usefulness and benefits of employing clinical linacs for nuclear physics experiments.

1 Introduction

The study of photon-induced nuclear reactions has been of interest over the years. The motivations for studying the interaction of photons with the nucleus are many, ranging from the fundamental nuclear structure studies to studying the inner working of a nuclear reactor and the inner processes in a star. Concerning nuclear reactors, photonuclear reactions contribute to the general performance of the reactor and their accurate understanding is a necessary part of any reactor core simulation. At the same time, the issues of nuclear astrophysics involve many reactions relating to photons, since, in a star, they are ubiquitous. In fact, photonuclear reactions are crucial steps in many of the nucleosynthesis processes generating the observed abundances of elements. Thus, many photonuclear reaction experiments are aimed at and motivated by astrophysical references to nucleosynthesis, see refs. [1–7] and references therein.

In addition, the photonuclear reactions have been frequently applied in photo-activation studies pertaining to various fields. This combination of basic research aimed at fundamental physics and applied research makes the photonuclear reaction quite interesting and facilitates active research in several fields. This activity is also on the increase as the availability of radiation sources increases and their cost decreases. For the study presented in this paper, the availability of a good radiation source was the main impetus for embarking on this research activity.

Photo-activation experiments involving linear accelerators have been performed at several institutions around the world, refs. [8, 9], most notably at specialized laboratories such as S-DALINAC at TU Darmstadt, refs. [10, 11], and ELBE in Forschungszentrum Dresden in Rossendorf, ref. [12]. However, a study in ref. [13] has shown how a non-specialized instrumentation such as a clinical linac can also be employed for such experiments. This idea is a departure from conventional approaches in which linear accelerators used for photonuclear experiments have been designed and commissioned with the sole use in nuclear physics experiments in mind.

[a] e-mail: haris@akdeniz.edu.tr

The concept of using an "off-the-shelf" linac, originally designed for a different purpose, is a novel idea. Although this idea is an attractive one, the original study presented in ref. [13] has not been followed up on and its impact has been very limited. In light of availability of clinical linacs —in Turkey alone there are over 200 such devices— it is clearly a wasted opportunity not to use them for research. Especially important is the potential contribution such devices can have on progress of experimental nuclear physics in developing countries. In developing countries access to specifically designed linacs is practically non-existent, whereas access to clinical linacs is often readily available. Thus either trying to obtain one such linac, after its duty cycle in medicine is over, or working closely with the local hospital, to utilize the linac still in us in its off-hours, presents a way how these device can help developing countries to contribute to the global nuclear physics knowledge development. It is important to note further that there has been a great expansion of available radiation sources in the form of clinical linacs not just in developing countries, but across the world.

The main aim of this work is to follow up on the original work of ref. [13] and revive this line of research. We will show how a repurposed clinical linac can produce solid nuclear physics experiments, and that it is possible even without a sophisticated specifically designed linac to obtain good quality data. What we intend to demonstrate is that nuclear physics experiments with a clinical linac are a viable concept and one that can be of value to the global science community.

For this purpose it is essential to choose an appropriate example where the opportunity for contribution can be clearly demonstrated. A kind of niche where limited budget experiments can contribute to the global knowledge. One such opportunity presents itself in cases where the measurements of basic nuclear quantities, such as transition energies and half-lives, have not been performed for several decades even in the case of elements near to the valley of stability. Hopefully by presenting an appealing and convincing example the viability of the concept will be clearly demonstrated contributing to its popularity.

In order to best illustrate the potential of clinical linacs in experimental nuclear physics, we have chosen to focus on zinc isotopes to study the transition energies and half-lives of isotopes created by photonuclear reactions. The choice of zinc as a target of bremsstrahlung photons produced by the clinical linac is motivated by several reasons. Mainly, we are interested in studying intermediate mass nuclei, especially those isotopes on the proton-rich side of the nuclear chart. In addition, the data for the ^{63}Zn isotope, the main focus of this study, and its β-decay product ^{63}Cu are nearly 40 years old, see ref. [14]. This is the second part of the motivation for this study, *i.e.* to revisit some of the experimental results obtained quite some time ago and not investigated again. The goal behind this choice is to improve the data accuracy thus illustrating what this and similar studies can accomplish. This work aims at demonstrating both the feasibility of photonuclear experiments with a clinical linac as well as to point out that there are isotopes, close to the valley of stability, whose reexamination is worthwhile. In the initial study presented in ref. [13] the second part of this motivation was not explored in detail. In addition, we would like to note that we have already had reasonable success with this approach in our preliminary study published in ref. [15].

The paper is organized as follows; in sect. 2 we give the properties of the clinical linac used in this study. Detector setup and the experimental procedure used are presented in sect. 3. The explanation of the data analysis and the presentation of the results are provided in sect. 4 and finally, we present our summary and conclusions in sect. 5.

2 Properties of the clinical linac

The photonuclear reactions by their very nature require a source of photons, energetic enough to excite the target nuclei. In our experiment, the photon source was a clinical electron linac. The linac was re-commissioned from its usual role in medical physics for the use in the study of photonuclear reactions. It should be noted that a pioneering study by ref. [13] demonstrated that these clinical linacs (cLINAC) have properties appropriate for use in photonuclear reactions. In fact, it was demonstrated that they even compare well with the linacs made specifically for physics experiments. And while our study has been conducted with a re-commissioned linac the study in ref. [13] was done while the linac was still in medical use. While the later arrangement is possible with some coordination and planing the former arrangement gives more freedom for conduction experiments.

In our setup, we have used a cLINAC SLI-25 manufactured by Philips Medical Systems (currently part of Elekta TM Synergy TM), as a bremsstrahlung photon source, shown in fig. 1. The accelerator's technical documentation can be found in ref. [16]. The cLINAC primary electron beam is generated by an electron gun with an energy of about 50 keV. The electron gun in SLI-25 is a diode design with a 400 Hz pulse repetition frequency. After injection into the linac's copper cavity, the electrons are accelerated by a radio-frequency wave with 3 GHz (2856 MHz), S-band. The copper cavity is a traveling wave design, where the power is injected at the beginning of the accelerator structure. Even though the linac is designed to operate at energies up to 25 MeV, the power is provided by the magnetron instead of the klystron, which is more common for such energies. The nominal power supplied by the magnetron is 2.5 MW at 4 MeV (low energies) and 5 MW at 25 MeV (high energies). As is usual, all steering and focusing of the beam is achieved by standard magnetic and electrostatic devices.

Fig. 1. Philips SLI-25 clinical linear electron accelerator of Elekta TM Synergy TM.

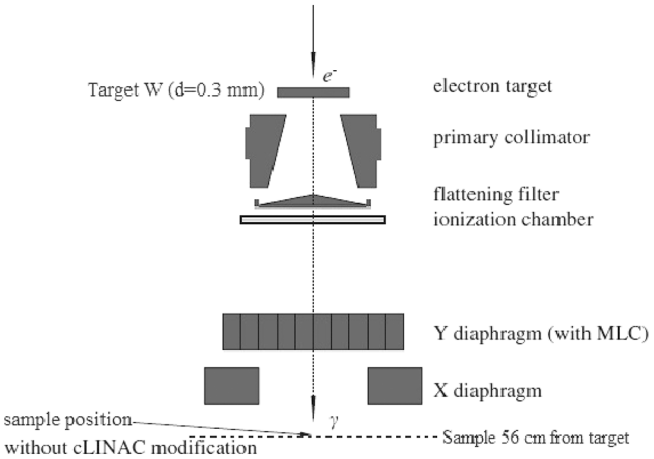

Fig. 2. Schematic view of the cLINAC.

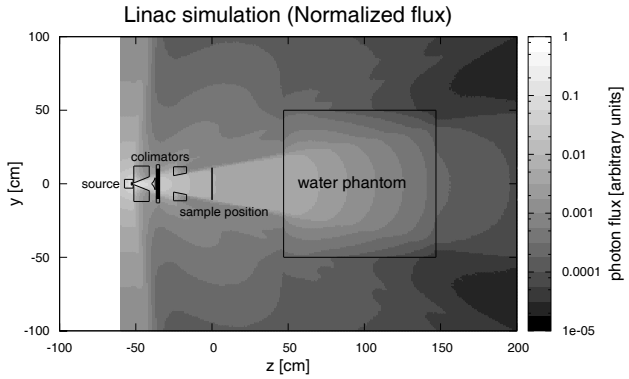

Fig. 3. Linac photon-flux distribution simulation normalized to the maximal flux.

After exciting the copper cavity, the beam is steered through 112.5° slalom-type magnetic and electrostatic devices before falling onto a high-Z element target, in our case, tungsten. The tungsten target is 0.3 mm thick and serves as an electron stopper and a bremsstrahlung photon source. Because the linac's original purpose was medical, *i.e.* for patient treatment, the bremsstrahlung photons are collimated and flattened with several filters placed as shown in fig. 2. The resulting photon beam is spatially uniform with no position dependence, *i.e.* the beam has the same intensity at the center as it has at the edges of the field. To further illustrate this, we show in fig. 3 a simulation of the photon flux created by the linac. As is evident in the figure the photon flux is flat across the sample position at 56 cm. For us, this is especially convenient as it avoids the necessity for complicated arrangements to create uniform sample irradiation. The focusing and collimation is a standard feature of all cLINACs, as it is paramount to maintain excellent spatial dose profile control when irradiating a patient. In fact, it is common to require dose knowledge to better than 3% accuracy. The dose and the dose spatial distribution are measured regularly as part of the standard linac performance monitoring.

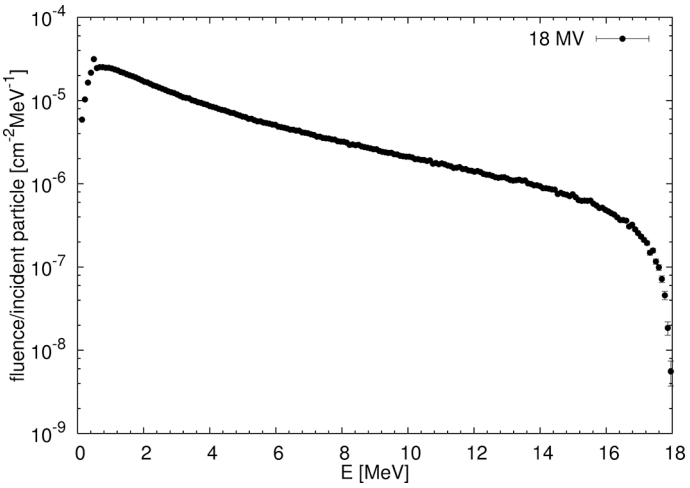

Fig. 4. EGS simulation of bremsstrahlung energy distribution from an electron beam accelerated over an 18 MV potential difference impacting on thick tungsten target in Philips SLI-25 clinical linac. The distribution shown is per incident electron.

Figure 3 shows a simulation of the photon flux produced by the linac. The figure shows the photon flux relative to the maximum flux in arbitrary units. It shows the location of the collimators and the flattening filter as well as their influence on the flux. Once the beam passes the flattening filter, which is of conic shape and much thicker in the center than at the edges, the beam loses any spatial dependence in intensity and becomes flat across the width of the filter. In addition, the collimators strongly reduce the beam intensity outside the focal area leading to a difference of several orders of magnitude in intensity inside and outside of the focal opening. After the flattening filter and the collimators the beam remains both flat and focused as it continues its trajectory. Once it reaches the sample target position at 56 cm, an area of approximately $20 \times 20\,\mathrm{cm}^2$, it still has a uniform beam profile. The scoring plane for the bremsstrahlung spectrum was placed at the surface of the water phantom at 100 cm downstream. At this distance the beam covers uniformly an area of $40 \times 40\,\mathrm{cm}^2$. Note that the surface of the water phantom was greater than $40 \times 40\,\mathrm{cm}^2$. Even as it travels through the phantom the beam still retains its uniformity to a very good degree. Although not used in the present experiments the collimators and the flattening filters can be used to create narrower or irregularly shaped field shapes.

Under all of these conditions, the question of bremsstrahlung energy distribution, which comes from the linac, becomes a quite complicated one due to presence of all the filters and collimators. A simulation of the photon energy distribution coming from the SLI-25 was performed using the BEAMnrc package, ref. [17]. The resulting distribution is shown in fig. 4. The distribution shown was calculated with an electron beam accelerated over an 18 MV potential difference impacting on a tungsten target of 0.3 mm thickness. As is usual, the distribution was calculated per incoming electron. For the estimation of the full flux, it is necessary to take into account the number of incident electrons. In our case, this number can be estimated from the dose delivered by the beam, 5 Gy/min, ref. [16], to be about 10^{11} electron/s. Combined with the simulation from BEAMnrc, this gives about 5×10^5 photons/(MeV cm^2 s) at $\bar{E} = 6$ MeV.

3 Detector set-up and experimental procedure

In the experiment, one zinc sample was placed immediately outside the cLINAC head at about 56 cm source to sample distance, see fig. 2. The sample in question was a zinc disk weighing 5 g with 5 mm diameter and 1 mm thickness. The sample was irradiated for about 35 min. The time was optimized such that a good count rate was achieved in the detector; the count rate was low enough not to cause pile up in the detector and yet high enough to observe several relatively weak peaks (intensity $\sim 0.05\%$). The sample was made primarily of zinc (67% by mass fraction), but it had several impurities, primarily magnesium, some aluminum, little iron and trace amounts of other elements. However, in the previous tests, we have already observed that the impurities did not show up in the spectrum. In addition, since no special effort was made to isotopically enrich the target, the presence of different zinc isotopes can be considered as those of their natural abundances (^{64}Zn - 49.17%, ^{66}Zn - 27.17%, ^{67}Zn - 4.04%, ^{68}Zn - 18.45% and ^{70}Zn - 0.61%).

After the irradiation, the sample was transported to the Physics Department of Akdeniz University, where the detector was located. The detector used is a high-purity germanium detector (HPGe). It is a p-type, coaxial, electrically cooled HPGe detector, placed in a well-shielded cavity. The shield is 10 cm thick lead with an inner surface covered by a 2 mm copper foil to reduce the Pb X-rays generated in the Pb shielding. The HPGe detector used is a gamma-ray spectrometer from AMETEK-ORTEC (GEM40P4-83) with 40% relative efficiency and resolution of 768 eV FWHM at 122 keV for ^{57}Co source and 1.85 keV FWHM at 1332 keV for ^{60}Co source ref. [18]. It is connected to a set of Nuclear Instrumentation Modules consisting of ORTEC preamplifier, bias supply, spectroscopy amplifier, analog-to-digital converter and a computer. Data acquisition was carried out with MAESTRO32 software. Through some trial

and error in preliminary studies with zinc, we came to the conclusion that the best setup of electronics and detector for this experiment is the one with 16830 channels and a channel step of about 0.18 keV/channel, giving about 3000 keV for the last channel and the maximum transition energy which can be observed.

The sample was placed in front of the detector about 10 min after the irradiation and γ-ray counting continued for three days. During the counting, spectra were automatically recorded at regular time intervals. Initially, those time intervals were short $\sim$ 3 s, designed to follow the short-lived isotopes, while the later ones became longer $\sim$ 20 min when focusing on longer-lived isotopes.

Immediately before counting, a set of calibration sources were measured. For calibration, we used two sets of sources. The point sources were supplied by the Çekmece Nuclear Research and Training Center (IAEA 1364-43-2) and contained Co-60, Na-22, Mn-54, Cd-109, Co-57, Cs-137 and Ba-133 isotopes. The second set is a soil sample provided by the Turkish Atomic Energy Authority (TAEK). It contained different natural radioactive isotopes (^{40}K, ^{226}Ra and ^{232}Th) with known activities. From this sample, we used only the strongest peaks for calibration.

After the γ-ray measurement of the sample was performed, an equivalently long natural background spectrum was recorded. Once the background spectrum was recorded, the experiment was concluded with a second measurement of the calibration sources. The aim of this second calibration-sources measurement was to check the stability of the electronics and the measurements. In this way, we were able to track any channel shift during the measurement and also, through combining the before and after calibration results, eliminate or at the very least reduce any systematic errors coming from the channel shift.

The process of photo-activation applies to all the nuclei for which the bremsstrahlung radiation exceeds the reaction threshold. In a way, it is reasonable to assume that all the processes that are physically possible are realized inside the sample. The neutron separation energies of the zinc isotopes are in the range from 7 to 12 MeV and the proton separation energies are in the range from 7.5 to 11.5 MeV. Given that the endpoint energy of our beam was 18 MeV, it is expected that all of the stable zinc isotopes will get activated. However, due to limitations of the experimental setup, not all γ-decays from zinc isotopes were observable or have been observed. The photonuclear reactions whose signatures we have observed in the spectrum are:

$$^{64}\mathrm{Zn} + \gamma \rightarrow {}^{63}\mathrm{Zn} + n, \tag{1}$$

$$^{66}\mathrm{Zn} + \gamma \rightarrow {}^{65}\mathrm{Zn} + n, \tag{2}$$

$$^{70}\mathrm{Zn} + \gamma \rightarrow {}^{69}\mathrm{Zn}^{*} + n, \tag{3}$$

$$^{68}\mathrm{Zn} + \gamma \rightarrow {}^{67}\mathrm{Cu} + p. \tag{4}$$

The most important limitation for this reduced list is the half-life of the created nuclei. It is because of this that we do not see evidence of ^{67}Zn since the half-life of ^{66}Cu is only 5.12 min. At the same time the half-life criteria works in our favor and we are able to observe a long-lived (13.76 h) isomeric state of ^{69}Zn.

Our experimental setup was not designed for direct observation of the above reactions, *i.e.* prompt gammas, thus we have to rely on the radioactive decay of the created nuclei and their end-stage γ-decays. The experiment was intended to observe the half-life of the radioactive nuclei produced and the transition energies of their daughter products, not to observe the levels of stable nuclei which are used as the targets. In this respect, we list the decay reactions which we studied:

$$^{63}\mathrm{Zn} \rightarrow {}^{63}\mathrm{Cu}^{*} + e^{+} + \nu, \tag{5}$$

$$^{65}\mathrm{Zn} \rightarrow {}^{65}\mathrm{Cu}^{*} + e^{+} + \nu, \tag{6}$$

$$^{69}\mathrm{Zn}^{*} \rightarrow {}^{69}\mathrm{Zn} + \gamma, \tag{7}$$

$$^{67}\mathrm{Cu} \rightarrow {}^{67}\mathrm{Zn}^{*} + e + \bar{\nu}. \tag{8}$$

Here too, we have yet another limitation as to what we can observe. As is noticeable the β-decay of ^{69}Zn is missing from the above list since it was not directly present in the observed gamma spectrum. The observational limitation here is the low branching ratio of the ^{69}Zn β-decay into the excited states of ^{69}Ga. Namely this β-decay goes, almost exclusively (99.998%), to the ground state of ^{69}Ga leaving no gamma transition to be observed by the detector.

In addition to the process of photonuclear reactions, explained above, it should be noted that there exists a small ambiguity in the reactions for a few of the cases presented. This ambiguity appears due to somewhat high endpoint energy of the bremsstrahlung spectrum. As can be noticed, at 18 MeV the photon energy is higher than the neutron separation energy for most elements. As such, it is expected that the radiation source and the collimation materials will become sources of neutrons. Therefore, some of the nuclei observed could have been produced in neutron-capture reactions. However, this source of neutrons as secondary particles is rather low and the processes of photonuclear reactions presented above are dominant. Therefore, for the results on which this work focuses, such small interferences are not of significance. Only for the cross-section determination can such issues play a role.

These neutrons coming from the radiator and the collimation materials in the head of the linac are of interest in medical therapy and can be measured. In our case we have measured the slow neutron flux as being close to 8000 neutrons/(cm^2 s) at 100 cm distance from the radiator. The measurement was performed in the center of the photon beam. However it is expected that the neutrons will have a similar presence even outside of the photon beam, since the radiator emits neutrons in all directions. In medical therapy with photons this presents a problem since it causes a non-negligible dose outside the intended area. Other treatment modalities with charged particle offer better dose profiles and less neutron leakage ref. [19,20].

4 Data analysis and results

The data acquisition was performed with MAESTRO software; however, due to its limitations peak analysis and energy calibration were performed with other programs. Peak analysis was performed with RadWare code developed for analysis of gamma-ray coincidence data, by David Radford of the Physics Division at Oak Ridge National Laboratory, ref. [21], while energy calibration was performed in ROOT developed by CERN group, ref. [22]. The motivation for using two different programs was to strike a balance between the desired accuracy and time consumption for the data analysis. At the end, the data were combined in a simple calculation sheet, giving the transition-energy value and the associated error.

Thus, all of the recorded sample and background spectra as well as the calibration spectra taken before and after the experiment were analyzed with the RadWare package. The strength of the RadWare package and its suitability for the analysis of spectra recorded with a HPGe detector lies in the fact that it fits a Gaussian, a skewed Gaussian, and a smoothed step function to any number of chosen peaks. In this way, we determine the centroids, areas and respective statistical errors of all peaks found in a spectrum.

The first step of the analysis was performed on the calibration data taken before and after the experiment. As is usual, the peak position in terms of channel, *i.e.* centroid, was obtained. The two calibrations were then combined taking into account both the errors obtained during the fit as well as the distance between them, ref. [23]. In this way, we obtained a unified determination of calibration-source peak centroids. These were paired with the corresponding transition-energy data taken from literature. The best example of this procedure is the Co-60 with its two peaks at 1173.237 ± 0.004 keV and 1332.501 ± 0.005 keV. The centroids and energies are fitted with the aid of ROOT and the energy calibration with accurate uncertainty for the fit parameters is obtained. In addition, the fitting subroutine provides the correlation between the fit parameters. We note that the ROOT fitting procedure takes into account both the uncertainties in energy as well as the centroid according to the effective variance method.

At this point, the question arises as to which is the appropriate fitting function for the energy calibration. Nominally, the energy calibration should be linear, but in practice it may not be. Thus, we tested linear, quadratic and cubic energy calibrations. In our case, the quality of the fit improved as we used higher order polynomials. In fact, the χ^2/n.d.f. for linear fit was 15.48, for quadratic 5.65 and cubic 1.41. Hence, we used the cubic fit for the energy calibration.

The propagation of error from the defining energy calibration equation $E = \sum_{i=0}^{3} a_i ch^i$ then takes all errors into account. Error of the fit parameters σ_{a_i}, covariance cov_{ij} or correlation cor_{ij} matrix and the errors of the centroid determination itself σ_{ch}. The error formula can then be written as

$$\sigma_E^2 = \sum_{i=0}^{3} \left(\frac{\partial E}{\partial a_i}\right)^2 \sigma_{a_i}^2 + 2\sum_{i=0}^{3}\sum_{j>i}^{3} \left(\frac{\partial E}{\partial a_i}\right)\left(\frac{\partial E}{\partial a_j}\right) \mathrm{cov}_{ij} + \left(\frac{\partial E}{\partial ch}\right)^2 \sigma_{ch}^2 \tag{9}$$

$$= \sum_{i=0}^{3} \left(\frac{\partial E}{\partial a_i}\right)^2 \sigma_{a_i}^2 + 2\sum_{i=0}^{3}\sum_{j>i}^{3} \left(\frac{\partial E}{\partial a_i}\right)\left(\frac{\partial E}{\partial a_j}\right) \mathrm{cor}_{ij}\sigma_i\sigma_j + \left(\frac{\partial E}{\partial ch}\right)^2 \sigma_{ch}^2. \tag{10}$$

With the calibration done, we proceed to determine the peak position in the measured zinc sample spectrum. In addition to the sample spectrum, we also determined the recorded peak position in the background spectrum and used it to discard the same peaks found in the sample spectrum. What remained was the centroid position information for the peaks, which could be assigned to the sample. The energy and uncertainty were calculated according to eq. (10) and are listed in table 1.

When we compared the energy results, from table 1, with the literature values, it was possible to assign these peaks to γ-ray transitions in specific isotopes. In fig. 5, we show the irradiated-sample spectrum without any background subtraction. The energy assignment of peaks is shown in the figure. All the unassigned peaks are either background peaks or sum and escape peaks. On the other hand, all the assigned peaks can be connected with the nuclei produced in the photonuclear reactions on zinc isotopes. Hence, it is safe to say that any elemental pollution we might have had in the sample did not show up in the spectrum in the form of an unidentifiable peak. In this way, we verify that our assumption of *de facto* working with a pure zinc sample was justified.

Table 1. Gamma-ray energies obtained in the present measurement by averaging the results of before and after calibration measurements compared to values found in the literature (NUDAT).

Ele.	E_{NUDAT}(keV)	σ_{NUDAT}	$\bar{E}$(keV)	σ_E	$\Delta = \lvert E_{\mathrm{NUDAT}}\text{-}\bar{E}\rvert$	$D = \sqrt{(\sigma^2_{\mathrm{NUDAT}} + \sigma^2_{\bar{E}})}$	Δ/D
^{63}Zn	449.93	0.05	449.942	0.017	0.012	0.05	0.24
^{63}Zn	669.62	0.05	669.69	0.03	0.07	0.06	1.17
^{63}Zn	742.25	0.10	742.18	0.03	0.07	0.10	0.70
^{63}Zn	962.06	0.04	962.09	0.04	0.03	0.06	0.50
^{63}Zn	1123.72	0.07	1123.80	0.07	0.08	0.10	0.80
^{63}Zn	1327.03	0.08	1327.11	0.10	0.08	0.13	0.62
^{63}Zn	1374.47	0.13	1374.41	0.08	0.06	0.15	0.40
^{63}Zn	1392.55	0.08	1392.56	0.08	0.01	0.11	0.09
^{63}Zn	1412.08	0.05	1412.16	0.11	0.08	0.12	0.67
^{63}Zn	1547.04	0.06	1547.16	0.12	0.12	0.13	0.92
^{63}Zn	2026.8	0.3	2026.70	0.18	0.10	0.4	0.25
^{63}Zn	2336.5	0.3	2336.4	0.2	0.1	0.4	0.25
^{63}Zn	2536.0	0.3	2535.9	0.3	0.1	0.4	0.25
^{63}Zn	2696.6	0.3	2696.5	0.4	0.1	0.5	0.20
^{67}Cu	184.577	0.010	184.63	0.06	0.05	0.06	0.83
^{69}Zn	438.634	0.018	438.601	0.017	0.033	0.025	1.32
^{65}Zn	1115.539	0.002	1115.51	0.06	0.03	0.06	0.50

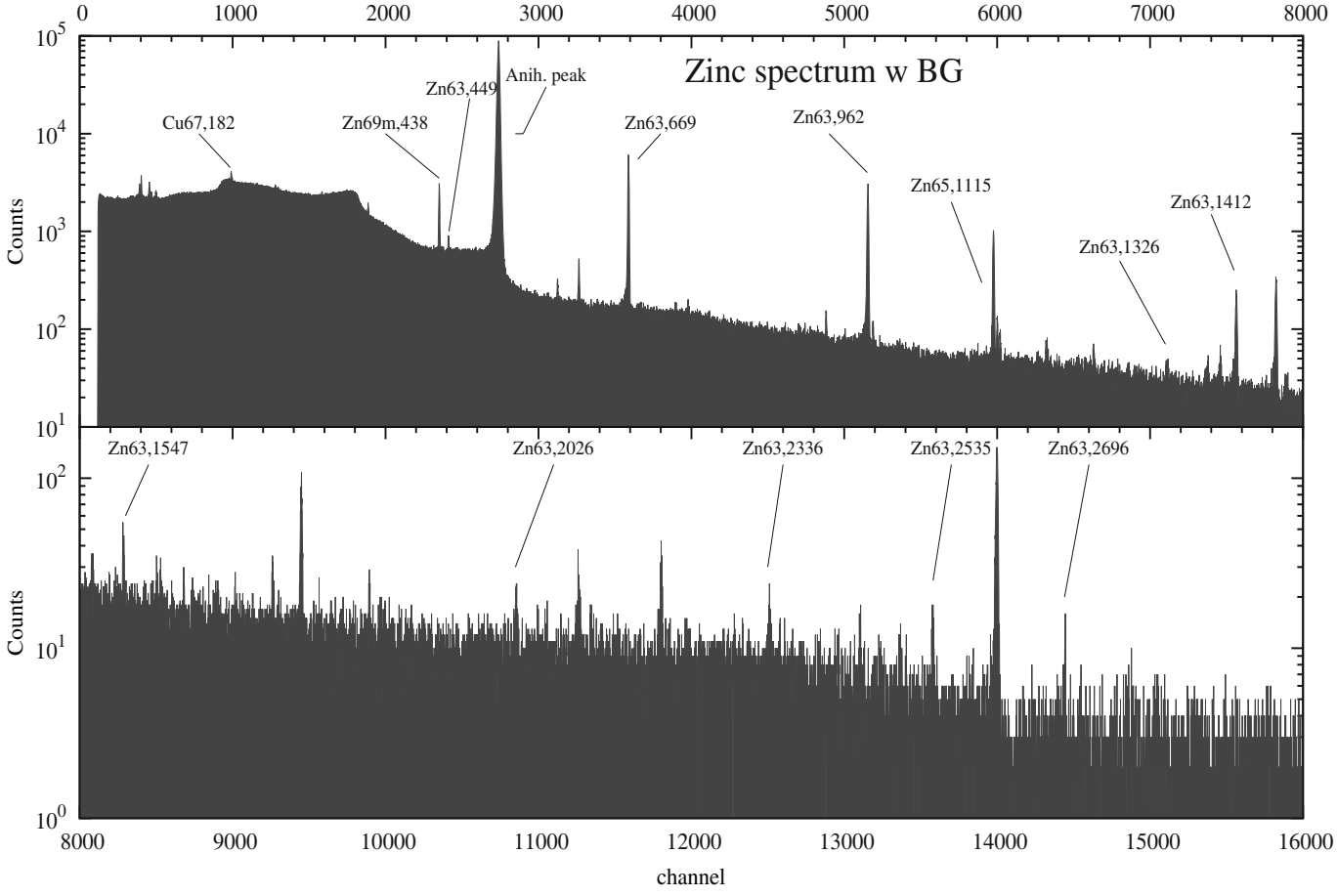

Fig. 5. Zinc sample spectrum with no subtractions, for the irradiated sample after 3 days of counting. Assigned peaks are labeled with their energy in keV based on the energy calibration, and also with the decaying isotope.

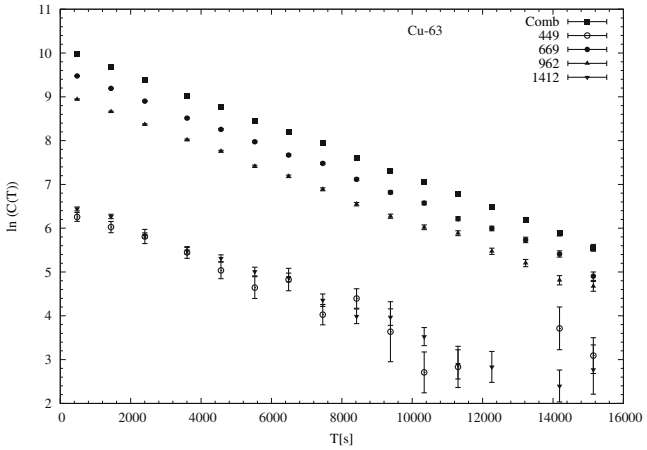

Fig. 6. Logarithmic time evolution of ^{63}Zn counts, as defined by eq. (11), for all transitions combined and separately for a few of the strongest ones.

Finally, the results obtained for the average energy and the combined variance are compared to literature values in table 1. The literature results quoted are taken from NUDAT and come from *Nuclear Data Sheets* publications, which, for these elements, are refs. [24–27]. In turn nuclear data sheets results are taken from individual publications: ref. [14] for ^{63}Zn decay, ref. [28,29] for ^{67}Cu decay, ref. [30,31] for ^{69}Zn decay, and ref. [32] and others for ^{65}Zn decay. In order to illustrate the quality of the agreement, we also show in table 1 how distant are our values from the literature ones. In addition, we show the ratio of the distance and the combination of our and literature uncertainties. It may be observed that the agreement is good. All the results agree within 1.5σ and most are within σ or better. Even if the uncertainties are not combined, but simply the larger of the two is taken, the agreement is still better than 2σ. At the same time, the results presented are of similar quality or better than the literature ones. The only exception being ^{65}Zn which is often used as a calibration standard and is measured to a very high accuracy.

In addition to the transition energies, the analysis performed provided information about counts and their time evolution. This information can be used to determine the half-life of the parent nucleus as the decay of the daughter levels are in secular equilibrium with the β-decay of the parent nucleus. Secular equilibrium is a very good assumption here since the half-lives of the states in question are orders of magnitude smaller than those of the parents. The only exception is the ^{69}Zn, which is an isomeric transition and is thus observed directly.

Usually the measurement of the half-life has involved the measurement of the decay as function of time and the fit to the activity with the exponential decay curve ($A(t) = A_0 \exp(-\lambda t)$). Also, a naive way would involve fits to the integral of the activity which is directly represented by the counts. However, fitting the peak in each consecutive step independently and then obtaining the half-life from these data is not appropriate since all the errors in each step are correlated, but the correlation is unknown. A better approach is to integrate the activity in equal-size time steps:

$$C(T) = \int_{T-\Delta T}^{T+\Delta T} A(t)\mathrm{d}t = C_0 e^{-\lambda T}\left(e^{\lambda \Delta T} - e^{-\lambda \Delta T}\right), \tag{11}$$

where $C_0 = A_0/\lambda$ and T is counting time. So long as the ΔT is a constant the function only depends on T exponentially just like activity.

In practical terms, this can be performed by taking independent spectra of length ΔT and restarting the count at the end of each time step. In this way, the counts obtained in two consecutive spectra are no longer correlated and the errors of the counts obtained in this way are independent of each other. Care should be taken to correct the counts obtained for dead time since while the detector is busy the sample is still decaying. In our case, this was a minor correction since only at the very beginning we had a small amount ($\sim 2\%$) of dead time.

In order to simplify the fit, logarithm of eq. (11) was used for fitting. In this case, one has a simple linear fit from which the decay constant λ is obtained. Once the value of the decay constant λ has been obtained, it is a straightforward matter to calculate the half-life $T_{1/2} = ln\,2/\lambda$.

Several examples of the counts dependence on time are shown in fig. 6. Only the best are shown, *i.e.* the strongest peaks, as well as the dependence of the sum count of all peaks. As could have been expected, a linear trend is quite evident and the error-bars are getting smaller for stronger peaks and earlier counting intervals. The remaining peaks were too weak to be fitted, *i.e.* the fitting procedure did not converge or gave very large uncertainties.

The summary of the fits to the function defined by eq. (11) and shown in fig. 6 is given in table 2. All of the errors listed in column 3 of table 2 are statistical only. As can be seen, the combined-counts fit offers the smallest error, but the two strongest peaks 669 and 962 are also quite good. When compared to the literature value of 38.47 ± 0.05 min, the combined-counts fit is quite decent. The remaining fits scatter noticeably around these values. However, all our values

Table 2. ^{63}Zn determined half-life from several transitions. These should be compared with NUDAT value of 38.47 ± 0.05 min.

Transition	$T_{1/2}$ [min]	$\sigma_{\text{stat.}}$	χ^2/n.d.f.
Combined	38.84	0.15	0.782
449	42.1	3.3	0.700
669	38.70	0.19	1.616
962	39.19	0.26	1.003
1412	39.2	1.2	0.977

are systematically higher than the literature value. This systematically higher result is likely the product of isotopic impurity of the sample, *i.e.* the counts of a single isotope are distorted by the presence of other ones. Unfortunately in the current experimental setup we can not eliminate this systematic uncertainty. Nevertheless, even with these pollution effects, the results are reasonable enough.

In addition to ^{63}Zn, we also fitted the γ-decay of ^{69}Zn isomeric transition and obtained 13.76 ± 0.18 h while the literature value is 13.76 ± 0.02 h in surprisingly good agreement with each other. Of the other two observed β-decays ^{65}Zn and ^{67}Cu, we were not able to fit their decay curves. The ^{65}Zn was not fit due to unfavorable ratio of its long half-life (244 d) and observation time (3 d). The ^{67}Cu was not fit due to the weakness of the signal. Like in the case of ^{63}Zn peaks, not listed in table 2, it had too big uncertainties to allow for a reasonable fit.

5 Summary and conclusion

In the experiment presented in this paper, we have investigated the spectra and half-lives of zinc isotopes produced through photonuclear reactions. The photonuclear reactions were induced by a bremsstrahlung photon beam generated by a linac. The particularly interesting point, in which we differed from previous such experiments, is that we have used a clinical linac. Our aim was to demonstrate the potential usefulness and the power of such machines, building on the pioneering work of ref. [13]. Our work was motivated by the availability of clinical linacs. Their presence is on the increase and after decommissioning from their use in medical treatments many are readily available to be used in research. In addition even linac still in medical use can be utilized for nuclear physics research, with some planing and good coordination with the medical institution operating the linac. Although this concept and the idea have been demonstrated in ref. [13], it has not created a trend of clinical-linac use in science. With this paper, we wished to bring this idea back into focus. Our aim was to show that a clinical linac can be a competitive tool in modern nuclear physics, and that it can be especially useful for laboratories such as ours, in the developing world, as an easy and accessible way of performing experiments.

We used a beam of 18 MeV endpoint energy, well above the proton and neutron separation energies of all zinc isotopes, activating all of them. However, our experiment was not designed to observe prompt gammas since it was offline. The elements, of which transitions from their nuclear levels were observed, are the decay products of radioactive elements created by the photo-activation of zinc. These transitions, as well as the half-lives of the parent nuclei, were the intended goal and in this respect the experiment performed was quite successful.

The experiment was separated into several parts, the crucial ones being the sample spectrum measurement, analysis and the calibrations. On the calibration side, we have made substantial efforts to understand the sources of errors and perform the analysis as accurate and complete as possible. We have performed and combined two calibrations, before and after the sample measurement, in order to account for channel drift during the course of the experiment. Such a procedure ensured that our data had a good robustness and was reliable. We have paid close attention to the fitted polynomial, choosing cubic as the best. For the sample spectrum, we paid close attention to any background contribution especially when considering the area under the peak, *i.e.* the counts. The second part of the analysis, the study of parent nuclei half-lives, was devoted to this.

As for the results themselves, we have demonstrated quite confidently that experiments such as ours improve the accuracy of transition energies. Indeed, we have obtained results, which are in good agreement with the literature values, but notably often with reduced uncertainties. Our main contribution can be seen in the case of ^{63}Zn, whose levels we have consistently determined to an accuracy level that is same or better than the one found in the literature. Granted the measurement to which we compared our data came from an experiment performed nearly 40 years ago, ref. [14], but this is exactly where we expect to improve on data from the literature. The results obtained and the setup of the experiment make the study presented in this paper quite interesting and a valuable contribution to the nuclear data set. In fact, we firmly believe that such clinical-linac-based studies on proton-rich nuclei can offer improvements of data in many intermediate-mass nuclei. In accordance with this idea we are currently investigating the application of the our experimental setup to other nuclei. Currently we have already performed several follow up measurements on nuclei such as Cl, Br, Sc, Ga, Sb and Pr and are in the process of analyzing the data. The initial results show much promise.

On the half-life side, our data are not as nearly impressive as for the transition energies. However, given the limitation of this study, it is still a good check of consistency. Furthermore, with the improvement of our experimental setup, primarily in target preparation and choice of nuclei, we are confident that further studies will offer better results on the half-lives as well. Obviously, increased experience in this kind of experiments will also contribute to improvement of results in the future. In fact our follow up experiment on other nuclei indicate a good improvement in the half-life determination.

We would like to thank the Akdeniz University Hospital for their generous support. The project has also received administrative support from the office of the Akdeniz University Rectorate. In addition, the project and its various contributors have been supported in part by TUBITAK-MFAG 114F220 and the 2216-Foreigner Research program. The authors would also like to thank Dr. Deniz Savran for very enlightening discussions regarding our data analysis in respect to half-life determination.

References

1. T. Webb, L. DeVeaux, F. Harmon, J. Petrisko, R. Spaulding *et al.*, in *Proceedings of the Particle Accelerator Conference* (2005) 2363.
2. B. Meyer, G. Mathews, W. Howard, S. Woosley, R. Hoffman, Astrophys. J. **399**, 656 (1992).
3. D. Lambert, Astron. Astrophys. Rev. **3**, 201 (1992).
4. T. Rauscher, A. Heger, R. Hoffman, S. Woosley, Astrophys. J. **576**, 323 (2002).
5. M. Arnould, S. Goriely, Phys. Rep. **384**, 1 (2003).
6. T. Hayakawa, N. Iwamoto, T. Shizuma, T. Kajino, H. Umeda *et al.*, Phys. Rev. Lett. **93**, 161102 (2004).
7. H. Utsunomiya, P. Mohr, A. Zilges, M. Rayet, Nucl. Phys. A **777**, 459 (2006).
8. H.R. Weller, M.W. Ahmed, H. Gao, W. Tornow, Y.K. Wu *et al.*, Prog. Part. Nucl. Phys. **62**, 257 (2009).
9. K. Masumoto, C. Segebade, *Photon Activation Analysis* (John Wiley & Sons, Ltd, 2006).
10. P. Mohr, J. Enders, T. Hartmann, H. Kaiser, D. Schiesser, S. Schmitt, S. Volz, F. Wissel, A. Zilges, Nucl. Instrum. Methods Phys. Res. A **423**, 480 (1999).
11. K. Sonnabend, D. Savran, J. Beller, M. Büssing, A. Constantinescu, M. Elvers, J. Endres, M. Fritzsche, J. Glorius, J. Hasper, J. Isaak, B. Löher, S. Müller, N. Pietralla, C. Romig, A. Sauerwein, L. Schnorrenberger, C. Wälzlein, A. Zilges, M. Zweidinger, Nucl. Instrum. Methods Phys. Res. A **640**, 6 (2011).
12. R. Schwengner, R. Beyer, F. Dönau, E. Grosse, A. Hartmann, A. Junghans, S. Mallion, G. Rusev, K. Schilling, W. Schulze, A. Wagner, Nucl. Instrum. Methods Phys. Res. A **555**, 211 (2005).
13. P. Mohr, S. Brieger, G. Witucki, M. Maetz, Nucl. Instrum. Methods A **580**, 1201 (2007).
14. A. Klaasse, P. Goudsmit, Z. Phys. **266**, 75 (1974).
15. I. Boztosun, H. Đapo, S.F. Ozmen, Y. Çeçen, M. Karakoç, A. Çoban, A. Cesur, T. Caner, E. Bayram, G.B. Keller, B. Kuçuk, A. Guvendi, M. Derman, D. Kaya, Turk. J. Phys. **38**, 1 (2014).
16. Electa, Elekta Digital Accelerator, Technical Training Guide (unpublished).
17. D.W.O. Rogers, B.A. Faddegon, G.X. Ding, C. Ma, J. We, T.R. Mackie, Med. Phys. **22**, 503 (1995).
18. MAESTRO, A65-b32-maestro-32-emulation-software.
19. R. Kaderka, D. Schardt, M. Durante, T. Berger, U. Ramm, J. Licher, C. La Tessa, Phys. Med. Biol. **57**, 5059 (2012).
20. C. La Tessa, T. Berger, R. Kaderka, D. Schardt, C. Körner, U. Ramm, J. Licher, N. Matsufuji, C.V. Dahlgren, T. Lomax *et al.*, Radiother. Oncol. **105**, 133 (2012).
21. D. Radford, Nucl. Instrum. Methods Phys. Res. A **361**, 297 (1995).
22. R. Brun, F. Rademakers, Nucl. Instrum. Methods Phys. Res. A **389**, 81 (1997).
23. A. Gun, K. Gupta, B. Dasgupta, *Fundamentals Of Statistics* (World Press, 2008).
24. B. Erjun, H. Junde, Nucl. Data Sheets **92**, 147 (2001).
25. E. Browne, J. Tuli, Nucl. Data Sheets **111**, 2425 (2010).
26. H. Junde, H. Xiaolong, J. Tuli, Nucl. Data Sheets **106**, 159 (2005).
27. C. Nesaraja, Nucl. Data Sheets **115**, 1 (2014).
28. R.A. Meyer, A.L. Prindle, W.A. Myers, P.K. Hopke, D. Dieterly, J.E. Koops, Phys. Rev. C **17**, 1822 (1978).
29. P. Yalcin, Y. Kurucu, Appl. Radiat. Isot. **62**, 63 (2005).
30. W. Zoller, G. Gordon, W. Walters, Nucl. Phys. A **124**, 15 (1969).
31. S. Raman, R.G. Couch, Phys. Rev. C **1**, 744 (1970).
32. R. Helmer, C. van der Leun, Nucl. Instrum. Methods Phys. Res. A **450**, 35 (2000).